CRYSTAL GROWTH & DESIGN

Article

pubs.acs.org/crystal

Leaf-like Tungsten Oxide Nanoplatelets Induced by Laser Ablation in Liquid and Subsequent Aging

Hongwen Zhang, Guotao Duan, Yue Li,* Xiaoxia Xu, Zhengfei Dai, and Weiping Cai*

Key Lab of Materials Physics, Anhui Key Lab of Nanomaterials and Nanotechnology, Institute of Solid State Physics, Chinese Academy of Sciences, Hefei 230031, P. R. China

Supporting Information

ABSTRACT: A facile and chemically clean method, pulsed laser ablation in liquid medium (LAL), was utilized to produce precursor solutions, and leaf-like tungsten oxide (WO_3) nanoplatelets were synthesized after sequential aging treatment of precursors. In this work, the effects of aging temperature, aging time, and pH value of precursor solutions have been investigated. The well-defined leaf-like WO_3 nanoplatelets can only be achieved by aging the pristine precursor solutions at room temperature (25 °C) for 48 h. In particular, when the pH value of precursor solutions was decreased lower than 1.0, the obtained products were hierarchical quasi-spheres composed of several nanoplates. The preparation method reported here shows a novel synthetic approach to control and adjust the morphology and crystallite size of the prepared WO_3 nanomaterials, which has potential applications in gas sensing, electrochromic devices, and photocatalysis.

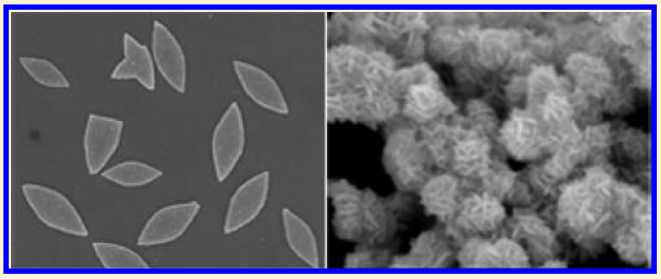

INTRODUCTION

Tungsten oxide (WO_3) is an important n-type semiconductor with a bandgap of 2.6 eV, and its bulk or film has been extensively studied owing to its wide applications in electrochromic devices,[1−3] gas sensors,[4−7] and catalysts.[8−10] Nanosized WO_3 materials show enhanced properties in these applications because of their lower dimensionality, higher surface area, and improved porosity. Nowadays, various WO_3 nanostructures, including nanowires,[6,11−13] nanobelts,[14−16] nanorods,[17−19] nanoplates,[20−23] and hierarchical micro-/nanostructures,[24−27] have been synthesized by deposition techniques and chemical routes. However, deposition techniques such as pulsed laser deposition (PLD), thermal deposition, etc. have the disadvantage of high cost and usually high vacuum dependence. Although chemical routes, such as sol−gel methods, ion-exchange approaches and hydrothermal means, possess advantages of simplicity and low cost, the unavoidably adulterated cations in the final products in these approaches show negative effects on the performances of designed functional devices.[28,29] Therefore, facile, green, and inexpensive approaches to prepare WO_3 nanomaterials with controlled characteristics are in urgent demand.

Pulsed laser ablation in liquid medium (LAL) is of particular interest and has been taken as an effective means to synthesize regular nanoparticles,[30,31] immiscible alloys,[32] metastable nanostructures,[33] and layer-structured[34,35] and even fullerene-like[36−38] nanomaterials. All these features are due to the ultrahigh temperature and ultrahigh pressure induced by reactions between pulsed laser and solid targets, which are realized at common ambient conditions. In addition, the chemical pureness (thus controlled doping) and freely selected solid targets and liquids enable us to fabricate diverse nanostructures with desired functions.[39,40]

Herein, we present a low-cost, simple, and chemically clean method to prepare leaf-like WO_3 nanoplatelets via the LAL method and subsequent aging. In this method, precursor solutions were first obtained by ablating pure tungsten target immersed in liquid medium of deionized water. Well-defined leaf-like tungstite nanoplatelets with a thickness of ca. 30 nm were then obtained after aging treatment of the as-prepared solutions at room temperature (RT, 25 °C) for 48 h. Besides leaf-like nanoplatelets, other nanostructures with different sizes and morphologies (quasi leaves and hierarchical structures, etc.) could also be obtained by changing the synthesis conditions, such as aging temperature, aging time, and pH value of precursor solutions. After calcination treatment at 500 °C for 2 h, all these tungstite architectures can be transformed to WO_3 via in situ dehydration, without obvious morphological changes. Also, a possible growth mechanism was put forward according to influences of those factors on morphology and grain size of obtained nanostructures. The WO_3 nanomaterials with different sizes and architectures prepared by LAL and subsequent aging may supply potential applications in constructing functional devices with good performances, such as electrochromic electrodes, chemical sensors, and so on.

Received: February 15, 2012
Revised: March 26, 2012
Published: April 15, 2012

   dx.doi.org/10.1021/cg300226r | *Cryst. Growth Des.* 2012, 12, 2646−2652

EXPERIMENTAL SECTION

First, a tungsten target (>99.9%, 45 mm × 10 mm × 1 mm) was polished with emery paper and ultrasonically rinsed with deionized water and ethanol for 1 h, respectively. The cleaned tungsten target was then immersed into a vessel filled with 30 mL of deionized water. A focused Nd:YAG laser operated at 10 Hz with a wavelength of 1064 nm and pulse duration of 10 ns vertically irradiated on the surface of tungsten target surrounded by deionized water. The diameter of laser beam focused on the target was ca. 2 mm. The tungsten target was irradiated with a power of 80 mJ/pulse for 120 min. The ablation medium was continuously stirred by a magnetic rotor during irradiation.

After irradiation, the as-prepared solutions were taken as precursors and aged at RT for 48 h. During the aging process, a series of color changes was observed from yellow brown (the time after ablation) to colorless (aged for about 5 h), then to white turbidness (aged for 20 h), and finally to colorless (yellow precipitation appearing at the bottom, aged for more than 24 h). The yellow precipitations were collected by centrifugation and rinsed with deionized water and ethanol three times, respectively. Yellow powder was obtained by drying the precipitations at 90 °C and subsequently annealed at 500 °C for 2 h for further investigation.

The morphology of the final yellow powder was observed by a field emission scanning electron microscopy (FE-SEM, FEI Sirion 200). The crystal structure of the samples was analyzed using an X-ray diffractometer (XRD, the Philips X'Pert) with copper Kα radiation (λ = 0.15406 nm) at room temperature. Transmission electron microscopy (TEM), high-resolution transmission electron microscopy (HR-TEM), and selected area electron diffraction (SAED) studies were performed on a JEM-200CX operated at 200 kV.

RESULTS

Precursor Solutions Prepared by LAL. When laser beam reaches the surface of tungsten target confined by deionized water, the induced ultrahigh temperature and ultrahigh pressure involved in tungsten plasma can enable complex reactions between tungsten species and water molecules. After ill-defined complex chemical reactions, isopolyanions of tungsten oxide are finally formed and they are easy to polymerize because of their instability.[41,42]

On the basis of that mentioned above and our experimental results, the formation process of precursor solutions can be briefly described as follows: (I) the high-temperature and high-pressure tungsten plasma is produced immediately at the solid–liquid interface when the pulsed laser arrives at the metal target; (II) the subsequent ultrasonic and adiabatic expansion of tungsten plasma leads to cooling down of the tungsten plume region and hence formation of small tungsten clusters;[18] (III) the chemically active tungsten clusters with still relatively high-temperature and high-pressure encounter the water molecules, which induces some complex chemical reactions, producing complex isopolytungstic acid; (IV) the isopolytungstic acid hydrolyzes, leading to the formation of the isopolyanions of tungsten oxide and realizing the acidification of solution;[41−43] (V) the formed isopolyanions are unstable and easy to polymerize in ill-defined degrees, resulting in the main suspension of precursor solutions.[42,44]

The ultracomplex process can be simplified and described by the following formulations,

$$W_{(bulk)} + h\upsilon \rightarrow W_{(plasma)} \quad (I)$$

$$W_{(plasma)} \rightarrow W_{(cluster)} \quad (II)$$

$$xW_{(cluster)} + (m+n)H_2O \rightarrow W_xO_m{\cdot}nH_2O + mH_2\uparrow \quad (III)$$

$$W_xO_m{\cdot}nH_2O \rightarrow 2nH^+ + [W_xO_{(m+n)}]^{2n-} \quad (IV)$$

$$y[W_xO_{(m+n)}]^{2n-} \rightarrow [W_{xy}O_{(m+n)y}]^{(2ny)-} \quad (V)$$

The freshly prepared precursors include isopolyanions of tungsten oxide and usually show a yellow brown color.[45] As the aging time increased, the initial isopolyanions of tungsten oxide aggregate and further polymerize, leading to the formation of bigger nanoparticles and showing white turbidity. When further increasing the aging time, these nanoparticles grow much bigger and are precipitated, demonstrating no color in the solutions.

Leaf-like WO_3 Nanoplatelets after Calcination Treatment. After the precursor solutions were aged at RT for 48 h, yellow precipitations appeared at the bottom of vessel. The precipitations were collected, rinsed, and calcined at 500 °C for 2 h for further characterization. A powder XRD pattern of the finally obtained products is shown in Figure 1a, and all peaks

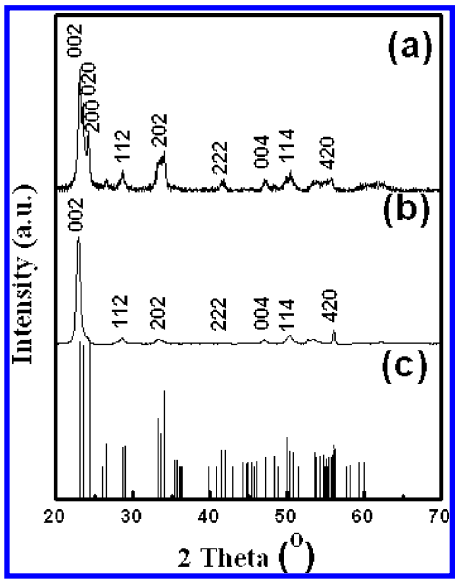

Figure 1. XRD patterns of the as-obtained yellow products prepared by the LAL method and subsequent aging treatment at RT (25 °C) for 48 h and annealed at 500 °C for 2 h. XRD patterns of the corresponding powder (a), film (b), and the standard pattern of monoclinic WO_3 (c), respectively.

can be readily indexed to the monoclinic WO_3 structures with the lattice parameters of a = 0.7297 nm, b = 0.7539 nm, c = 0.7688 nm and a space group of $P21/n$ (Figure 1c, JCPDS No. 43-1035). Although the pattern was acquired from powder samples, the relatively enhanced (002) reflection suggests that the products show a preferential orientation of the (002) crystal plane. To further confirm the preferential information, the XRD analysis (Figure 1b) of a film obtained by spin-coating of above WO_3 powders was performed. It clearly depicts an outstanding intense (002) reflection peak compared with the standard pattern and verifies that the obtained WO_3 structures have a preferred orientation in (002).

An FE-SEM observation with low magnification clearly indicates that the finally obtained WO_3 powders consist of well-dispersed nanoplatelets with dimensions ranging from a few tens of nanometers to several micrometers, as demonstrated in Figure 2a. Figure 2b displays some typical nanoplatelets in a higher magnification, showing leaf-like morphologies with

dx.doi.org/10.1021/cg300226r | Cryst. Growth Des. 2012, 12, 2646–2652

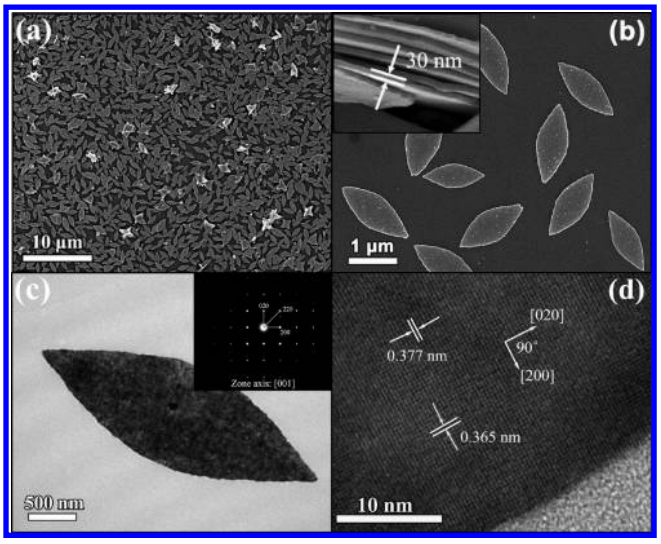

Figure 2. FE-SEM and TEM images of finally obtained WO_3 products prepared by LAL and subsequent aging treatment at RT for 48 h and annealed at 500 °C for 2 h. FE-SEM images at a low (a) and a high (b) magnification (the inset in (b) shows a top view from lateral sides, indicating a thickness of ca. 30 nm). TEM (c) and HR-TEM (d) images of an isolated WO_3 leaf. The inset in (c) shows the corresponding SAED pattern of the isolated nanoplatelet.

planar dimensions of ca. 1.8 and 0.6 μm in length and width, respectively, and a platelet thickness of approximately 30 nm (observed from side view, inset in Figure 2b). Figure 2c shows a low magnified TEM image of an isolated WO_3 nanoplatelet with the same size range, and its corresponding SAED pattern (inset in Figure 2c) exhibits highly uniform and ordered diffraction spots, revealing its single crystal nature. The diffraction patterns can also be indexed to monoclinic WO_3 along the [001] zone axis. A typical HR-TEM image of an edge of the isolated WO_3 nanoplatelet is shown in Figure 2d. The clear 2D ordered lattice structure indicates that the nanoplatelet is well crystalline. The interplanar distance values of 0.365 and 0.377 nm can be readily assigned to the (200) and (020) crystal planes of the monoclinic WO_3 phase (JCPDS No. 43-1035), respectively. One also finds that there exists the high consistency of the angle (90°) between the [200] and [020] directions with the crystallographic data.

The above analysis indicates that the finally calcined yellow powders, prepared by LAL and aging (RT, 48 h), are well-crystallized WO_3 nanoplatelets with leaf-like morphologies and a [002] preferred orientation normal to the surface of the nanoplatelets.

Intermediate Products after Aging without Calcination. Intermediate products, yellow precipitations derived from aging process of precursor solutions without calcination treatment, were also characterized by FE-SEM, XRD, etc. Figure 3a shows FE-SEM image of precipitations dried at 90 °C for 2 h. It shows that these intermediate products are also leaf-like nanoplatelets, and no obvious changes exist in morphology characteristics compared with observations after calcination treatment at 500 °C (Figure 2a,b), indicating a morphological inheritance from intermediate ones after calcination. The XRD pattern of the films composed of intermediate products dried at 90 °C for 2 h is shown in Figure 3b, and all peaks have been indexed to orthorhombic tungstite (Figure 3c, JCPDS No. 84-0886). Additionally, the XRD pattern demonstrates a highly strong intensity peak at 16.5° corresponding to the (020) plane,

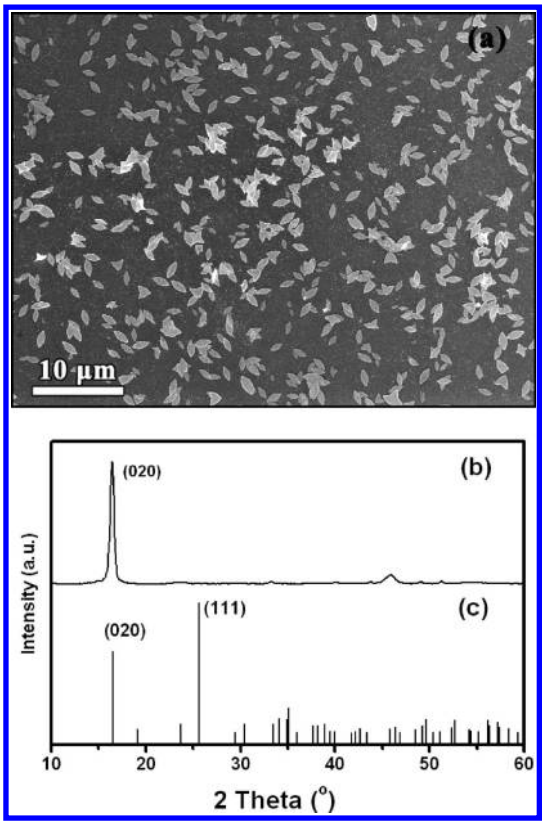

Figure 3. FE-SEM image (a) of intermediate products dried at 90 °C for 2 h and their XRD pattern (b) of films prepared by spin-coating method. Standard pattern (c) of orthorhombic tungstite (JCPDS No. 84-0886), indicating that the intermediate products own an intense preferred orientation in (020).

revealing that the intermediate products dried at 90 °C are orthorhombic tungstite owning preferred orientation in (020).

Transformation from (Hydrated) Tungstite to WO_3. As mentioned above, the monoclinic WO_3 nanostructures with leaf morphologies were derived from intermediate products, orthorhombic tungstite, via calcination treatment. In present work, we also investigated the phases at other drying temperatures, that is, RT and 60 °C, to know the detailed information about other possible intermediate products.

The XRD pattern of products dried at RT indicates a monoclinic hydrated tungstite ($H_2WO_4{\cdot}H_2O$, JCPDS No. 18-1420) with a preferred orientation of [010], whereas XRD pattern acquired from the powders dried at 60 °C gives evidence for coexistence of two phases, that is, a complex of monoclinic $H_2WO_4{\cdot}H_2O$ and orthorhombic H_2WO_4 (see Figure S1 in the Supporting Information).

Therefore, the finally obtained monoclinic WO_3 leaf-like nanoplatelets were acquired by dehydration step by step in drying and calcination processes without obvious morphological changes. And the evolution of preferred orientation from [010] (monoclinic $H_2WO_4{\cdot}H_2O$ and orthorhombic H_2WO_4) to [001] (monoclinic WO_3) can be simply explained by crystallographic topotaxy in the dehydration process,[23,46] as illustrated in Figure 4.

On the basis of the above facts, the evolution from [010] oriented $H_2WO_4{\cdot}H_2O$ to [001] oriented WO_3 can be expressed as follows,

dx.doi.org/10.1021/cg300226r | Cryst. Growth Des. 2012, 12, 2646−2652

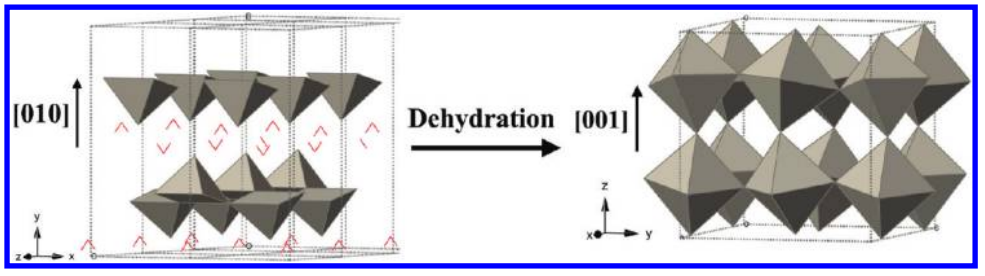

Figure 4. Schematic illustration of the evolution from [010] oriented orthorhombic tungstite to [001] oriented monoclinic tungsten oxide by dehydration process.

$$2H_2WO_4\cdot H_2O[010] \xrightarrow[60\ ^\circ C]{\text{partial dehydration}} H_2WO_4[010] + H_2WO_4\cdot H_2O[010] + H_2O\uparrow$$

$$H_2WO_4\cdot H_2O[010] \xrightarrow[90\ ^\circ C]{\text{dehydration}} H_2WO_4[010] + H_2O\uparrow$$

$$H_2WO_4[010] \xrightarrow[500\ ^\circ C]{\text{dehydration}} WO_3[001] + H_2O\uparrow$$

As a result, it is reasonable to take (hydrated) tungstite as a discussed target instead of WO_3 when needed.

DISCUSSION

1. Influence Factors. *Aging Time.* Different aging times were applied to the precursor solutions prepared by LAL at RT to monitor the formation process of leaf-like (hydrated) WO_3 nanostructures, which can also be taken as the influence of aging time, as illustrated in Figure 5. All the samples obtained by aging treatment for different times were treated at 90 °C for 2 h before further characterization.

After the LAL process was finished, the TEM sample was immediately made from the freshly prepared precursor solutions to characterize the initial products without aging. As illustrated in Figure 5a, when no aging treatment was applied, the products consist of irregular particles with an average size of 5 nm. And the corresponding SAED (inset of Figure 5a) shows a typically amorphous pattern. But when aged for 4 h, some aggregated nanoparticles appear and their SAED pattern, from which three discriminable diffraction rings correspond to (121), (031), and (121) planes of orthorhombic tungstite respectively, indicates that crystallites exist in the aggregation (Figure 5b and its inset). A higher resolution TEM (Figure 5c) illustrates a 10 nm-sized crystallite with clear ordered lattice. The measured interplanar distance of 0.287 nm most likely corresponds to the (031) crystallographic plane of orthorhombic tungstite. For an aging time of 10 h, the crystallite size grows larger (ca. 20 nm), and the products appear to be dispersed crystallized nanoparticles with well-defined edges (Figure 5d). The SAED (inset of Figure 5d) confirms its tungstite phase and clearly indicates an improved crystalline of nanoparticles compared with that of products aged for 4 h. When aged for 24 h (Figure 5e), the products consisting of leaf-like nanoplatelets with an average size of ca. 0.6 μm and an aspect ratio of ca. 2.3 were obtained. When the aging time increased to 60 h, both the particle size (ca. 1.8 μm) and the aspect ratio (ca. 2.8) of the nanoplatelets became larger and the edges of leaves demonstrated a phenomenon of linearization (Figure 5f).

These results indicate that, as the aging time increased, the crystallization degree of the obtained nanostructures is

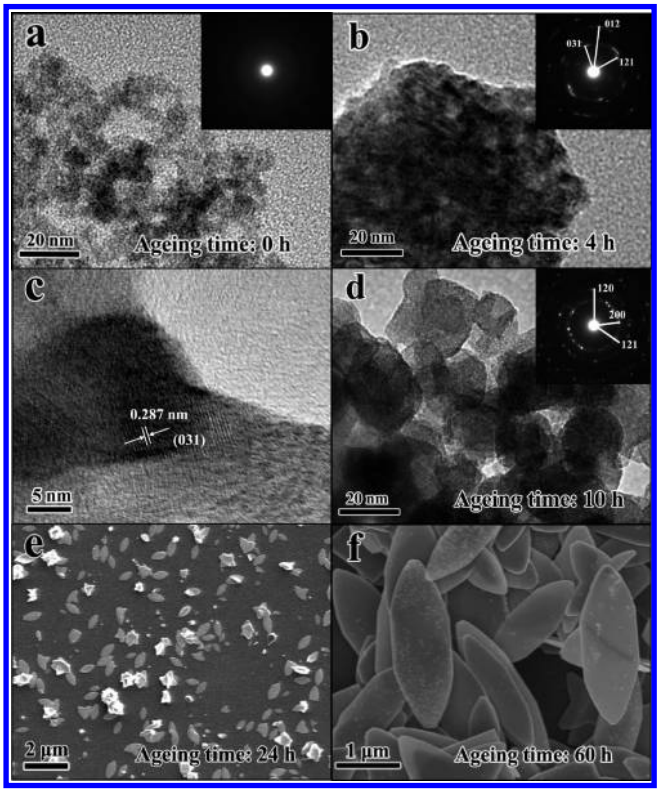

Figure 5. TEM or FE-SEM images of hydrated tungsten oxide obtained at an aging time of 0 h (a), 4 h (b, c), 10 h (d), 24 h (e), and 60 h (f). All samples were dried at 90 °C for 2 h before characterization. Insets of (a), (b), and (d) are corresponding SAED patterns.

improved gradually and the grain size becomes larger, accompanied by morphological changes from irregularly shaped amorphous nanoparticles, nanosheets with edges and corners, to well-defined leaf-like morphologies, which induces the color changes of the solution. The evolution of crystallization and grain size indicates that the formation of tungstite leaves occurs in two stages, that is, nucleation to form a nucleus and subsequent growth of the nucleus to a larger size.

Aging Temperature. Figure 6 exhibits the morphologies of the products obtained by aging precursor solution at 10 and 0 °C for 48 h, respectively, while keeping other experimental conditions unchanged. It depicts that the similar leaf-like morphologies were achieved. Coupled with the results aged at 25 °C, the aspect ratios of the nanoplatelets were approximately 3, 1.7, and 1.4 for aging temperature of 25, 10, and 0 °C, respectively. It shows that the aspect ratio of the "leaf" decreased markedly as the environmental temperature

dx.doi.org/10.1021/cg300226r | Cryst. Growth Des. 2012, 12, 2646−2652

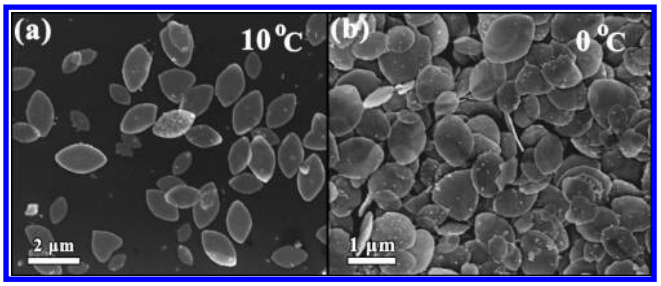

Figure 6. FE-SEM images of products obtained by LAL and aged at temperatures of 10 °C (a) and 0 °C (b), respectively.

decreased in the aging process, indicating a temperature-dependent effect.

Precursor Solution's pH Value. After irradiation for 2 h, the pH value of the freshly obtained precursor solution was about 3.0. After aging treatment of the as-prepared precursor solutions for 48 h at RT, we can obtain the well-defined leaf-like (hydrated) WO_3 nanostructures. In this work, we also investigated the effect of the acidity of precursor on morphologies of final products in the aging process. The freshly obtained precursor solutions were acidified to −0.6, 1.0, and 2.0 of pH values, respectively, by slowly adding sulfuric acid drop by drop. After aging for 48 h at RT, the precipitations were collected by centrifugation and rinsed with ethanol and deionized water several times. The obtained powder was dried at 90 °C for 2 h for further characterization.

Figure 7 shows the FE-SEM images of products obtained at varying pH conditions. Strikingly, unlike the nanostructures prepared without acidification treatment (pH = 3.0), the products prepared at pH = −0.6 and 1.0 turned out to be hierarchical nanoarchitectures (Figure 7a,c). When the pH value is −0.6, hierarchical particles with a size from 90 to 120 nm are obtained, which are composed of many tiny nanoplatelets with a uniform thickness of ca. 5 nm and a lateral size of about 50 nm (inset of Figure 7a). Figure 7b also shows a low-magnified TEM image of several hierarchical particles, regardless of ultrasonically dispersion before TEM observation. When the pH increased to 1.0, similar hierarchical structures were also observed (Figure 7c), while dimensions of both hierarchical particles and the corresponding primary building nanoplates became slightly larger. We conclude that the primary building nanoplates aggregated together to form bigger particles as the pH decreased. However, when the pH increased to 2.0, a significantly different morphology of product, leaf-like nanoplatelets, started to be formed again (Figure 7d), just as the results of products prepared without acidification treatment. The average dimension of leaf-like nanoplatelets prepared in this condition was ca. 1.3 μm, which was much larger than hierarchical particles.

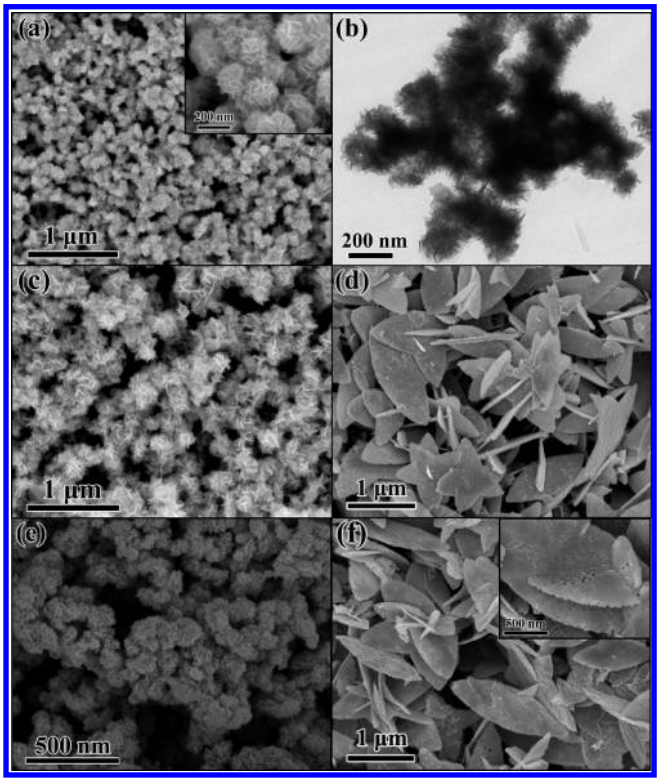

Figure 7. FE-SEM and TEM images of products obtained by acidifying precursor solutions to varying degrees, typically, pH = −0.6 (a, b), 1.0 (c), and 2.0 (d). Panels (e) and (f) are FE-SEM images of products after annealing treatment of (a) and (d) at 500 °C, respectively.

These results indicate that the hierarchical nanoarchitectures composed of several nanoplates were formed at lower pH (<1.0), while only leaf-like nanoplatelets were obtained when the pH was larger than 2.0. Also, the particle sizes were increased apparently with a larger pH value.

After annealing at 500 °C for 2 h, all samples obtained at different pH values were transformed to WO_3 and their morphologies were almost retained besides a little change. After calcinations, the hierarchical nanostructures became porous architectures composed of smaller nanoparticles (Figure 7e), but not previous nanoplates, while the leaf-like nanoplatelets obtained at pH = 2.0 demonstrated some nanopores on their surfaces (Figure 7f and its inset).

2. Formation Mechanisms of Leaf-like WO_3 Nanoplatelets. Derived from the influences of aging time on crystallization and grain size of obtained products, the formation of leaf-like (hydrated) tungsten oxide showed typical processes of nucleation and subsequent growth of nucleus. When precursors were aged, those processes were induced by further polymerization and aggregation of tungsten oxide isopolyanions. Also, the results of other influence factors indicate that the aging temperature has almost no effect on the morphology but aspect ratio, while the pH value of precursor solutions show crucial effects. It is concluded that the well-defined leaf-like tungsten oxide nanoplatelets can only be achieved at specific conditions, that is, appropriate aging time (48 h), proper aging temperature (RT, 25 °C), and suitable $[H^+]$ concentration (pH of approximately 3.0). It has been demonstrated that the finally prepared tungsten oxide nanomaterials were obtained by in situ dehydration of intermediate products (hydrated tungstite) step by step without obvious morphology changes during the drying and annealing process. As a result, the most fundamental understanding for formation of leaf-like tungsten oxide nanoplatelets can be obtained by investigating how the hydrated tungsten oxide was formed. For simplicity, we take tungstite (H_2WO_4) as the target.

It is helpful to understand the formation of H_2WO_4 nanoplatelets when its crystal structure is taken into account. As can be shown from the unit cell of tungstite (Figure 8), the central tungsten atom is surrounded by six oxygen atoms to form a W−O octahedron through covalent bond interaction.[47] The W−O octahedrons in the $a-c$ plane connect with each

dx.doi.org/10.1021/cg300226r | Cryst. Growth Des. 2012, 12, 2646−2652

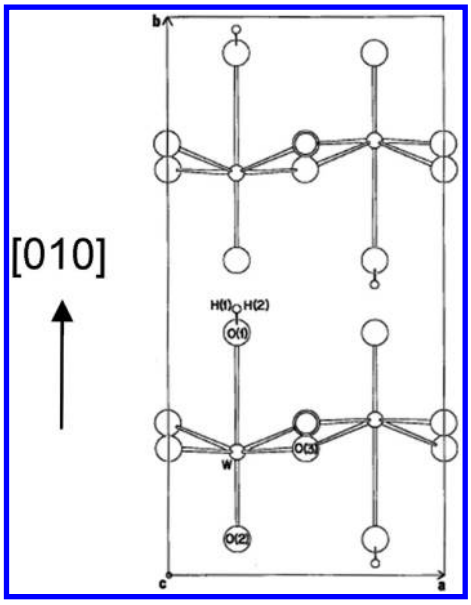

Figure 8. Schematic illustration of the unit cell of tungstite.

other by corner-sharing to form an infinite layer. Hydrogen bond interaction connects adjacent layers and thus a bulk form is built up.[48,49] Obviously, the relatively weaker interaction between adjacent layers must restrict their stacking along the *b* axis, leading to the formation of sheet-like tungstite with [010] preferred orientation. When dehydrated to monoclinic tungsten oxide, the sheet morphology was inherited with an inevitable [001] orientation.

Schematic illustration for the growth mechanisms of the prepared tungstites obtained at the mentioned specific and varying experimental conditions is shown in Figure 9. On the basis of the effects of pH values of precursor solutions, higher $[H^+]$ concentrations would induce higher nucleation velocity, leading to products with smaller grain size. For specific conditions (pristine precursor solution, aged for 48 h at RT), the $[H^+]$ concentration was relatively low and thus crystal growth was outstandingly predominant. Therefore, the nuclei with limited quantity began to grow slowly by taking surrounding tungsten oxide isopolyanions as starting materials. According to the Bravais law, the faces with high reticular density tend to be the exposed surfaces during crystal growth; that is, direction along which interplanar distance is larger has a lower growth rate. For orthorhombic tungstite, the interplanar distances in the $a-c$ plane have an order of $d(100) > d(001)$. As a result, the difference of crystal growth rate between the two vertical directions ensures that the obtained nanoplatelets have an aspect ratio not equal to 1, resulting in leaf-like nanoplatelets with curved edges (Figure 9a). With deviation from the specific conditions, diverse morphologies were achieved. When the aging process continued, the leaf-like nanoplatelets grew larger and the edges began to linearize gradually and had a tendency to form a rectangle (Figure 9b). As the aging temperature decreased, the growth rate along different directions was affected in a diverse extent, leading to leaf-like nanoplatelets with a changed aspect ratio (Figure 9c). When the pH value of the precursor solution was lower than 1.0, the initial crystal nuclei were formed quickly in large amount and began to grow larger gradually. To reach a minimization of surface energy, the neighboring nanosized particles tended to aggregate together to form hierarchical

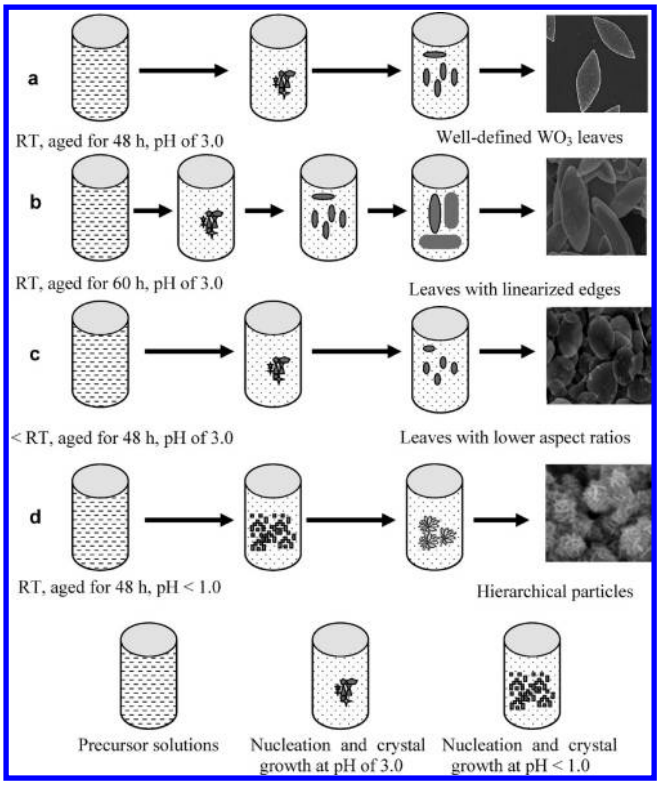

Figure 9. Schematic illustration for the growth mechanisms of the prepared (hydrated) tungstites obtained at varying experimental conditions.

architectures (Figure 9d). But when pH increased up to 2.0, the amount of initial crystal nuclei was limited and crystal growth was predominant. As a result, the size of particle was large enough to keep stable, resulting in isolated leaf-like nanoplatelets.

CONCLUSION

In summary, we have described a facile and chemically clean approach to produce leaf-like tungsten oxide nanoplatelets and characterized the resultant nanostructures by FE-SEM, TEM, SAED, and XRD to determine the morphologies and crystal structures. The leaf-like tungsten oxide nanoplatelets were prepared via aging treatment of the precursor solutions obtained by LAL of a tungsten target. By altering experimental conditions, we conclude that only at a proper aging temperature (25 °C), appropriate aging time (48 h), and suitable pH value (approximately 3.0) can the well-defined leaf-like tungsten oxide nanoplatelets be achieved, and when decreasing the pH value of the precursor solutions lower than 1.0, quasi-spheres consisting of several nanoplates were obtained. We proposed that the formation of nanoplatelets with preferred orientation were governed by the intrinsic crystal structure of (hydrated) tungstite, which shows W−O octahedron layers connected by hydrogen bonds to form three-dimensional structures. The mentioned method of producing tungsten oxide nanostructures with controllable morphologies and grain sizes may find potential applications in gas sensing, electrochromic devices, and photocatalysis.

dx.doi.org/10.1021/cg300226r | *Cryst. Growth Des.* 2012, 12, 2646−2652

■ ASSOCIATED CONTENT

Supporting Information

Film and powder XRD patterns of products dried at RT (25 °C) and 60 °C for 2 h. This material is available free of charge via Internet at http://pubs.acs.org.

■ AUTHOR INFORMATION

Corresponding Author

*E-mail: yueli@issp.ac.cn (Y.L.); wpcai@issp.ac.cn (W.C.).

Notes

The authors declare no competing financial interest.

■ ACKNOWLEDGMENTS

This work is financially supported by the National Basic Research Program of China (973 Program, Grant No. 2011CB302103), Recruitment Program of Global Experts (C), Natural Science Foundation of China (Grant Nos. 50831005, and 10974203), and Anhui Provincial Natural Science Funds for Distinguished Young Scholar (Grant No. 1108085J20).

■ REFERENCES

(1) Baeck, S. H.; Choi, K. S.; Jaramillo, T. F.; Stucky, G. D.; McFarland, E. W. *Adv. Mater.* **2003**, *15*, 1269−1273.

(2) Lee, D. H.; Kim, S. K.; Park, S. N.; Park, H. S.; Lee, J. Y.; Choi, S. K. *Appl. Opt.* **2009**, *48*, 37−42.

(3) Niklasson, G. A.; Granqvist, C. G. *J. Mater. Chem.* **2007**, *17*, 127−156.

(4) Penza, M.; Martucci, C.; Cassano, G. *Sens. Actuator B* **1998**, *50*, 52−59.

(5) Li, X. L.; Lou, T. J.; Sun, X. M.; Li, Y. D. *Inorg. Chem.* **2004**, *43*, 5442−5449.

(6) Polleux, J.; Gurlo, A.; Barsan, N.; Weimar, U.; Antonietti, M.; Niederberger, M. *Angew. Chem., Int. Ed.* **2006**, *45*, 261−265.

(7) Liu, Z. F.; Miyauchi, M.; Yamazaki, T.; Shen, Y. B. *Sens. Actuator B-Chem.* **2009**, *140*, 514−519.

(8) Kominami, H.; Yabutani, K.; Yamamoto, T.; Kara, Y.; Ohtani, B. *J. Mater. Chem.* **2001**, *11*, 3222−3227.

(9) Cui, X. Z.; Zhang, H.; Dong, X. P.; Chen, H. R.; Zhang, L. X.; Guo, L. M.; Shi, J. L. *J. Mater. Chem.* **2008**, *18*, 3575−3580.

(10) Zhao, Z. G.; Miyauchi, M. *Angew. Chem., Int. Ed.* **2008**, *47*, 7051−7055.

(11) Song, X. C.; Zheng, Y. F.; Yang, E.; Wang, Y. *Mater. Lett.* **2007**, *61*, 3904−3908.

(12) Zhang, J.; Tu, J. P.; Xia, X. H.; Wang, X. L.; Gu, C. D. *J. Mater. Chem.* **2011**, *21*, 5492−5498.

(13) Gu, G.; Zheng, B.; Han, W. Q.; Roth, S.; Liu, J. *Nano Lett.* **2002**, *2*, 849−851.

(14) Song, X. C.; Zhao, Y.; Zheng, Y. F. *Mater. Lett.* **2006**, *60*, 3405−3408.

(15) Chen, D. L.; Sugahara, Y. *Chem. Mater.* **2007**, *19*, 1808−1815.

(16) Wang, H.; Quan, X.; Zhang, Y.; Chen, S. *Nanotechnology* **2008**, *19*, 065704.

(17) Lee, K.; Seo, W. S.; Park, J. T. *J. Am. Chem. Soc.* **2003**, *125*, 3408−3409.

(18) Xiang, Q.; Meng, G. F.; Zhao, H. B.; Zhang, Y.; Li, H.; Ma, W. J.; Xu, J. Q. *J. Phys. Chem. C* **2010**, *114*, 2049−2055.

(19) Guo, C.; Yin, S.; Huang, Y.; Dong, Q.; Sato, T. *Langmuir* **2011**, *27*, 12172−12178.

(20) Sadek, A. Z.; Zheng, H. D.; Breedon, M.; Bansal, V.; Bhargava, S. K.; Latham, K.; Zhu, J. M.; Yu, L. S.; Hu, Z.; Spizzirri, P. G.; Wlodarski, W.; Kalantar-zadeh, K. *Langmuir* **2009**, *25*, 9545−9551.

(21) Su, X.; Xiao, F.; Li, Y.; Jian, J.; Sun, Q.; Wang, J. *Mater. Lett.* **2010**, *64*, 1232−1234.

(22) Ma, J.; Zhang, J.; Wang, S.; Wang, T.; Lian, J.; Duan, X.; Zheng, W. *J. Phys. Chem. C* **2011**, *115*, 18157−18163.

(23) Chen, D. L.; Gao, L.; Yasumori, A.; Kuroda, K.; Sugahara, Y. *Small* **2008**, *4*, 1813−1822.

(24) Ma, Y. L.; Zhang, L.; Cao, X. F.; Chen, X. T.; Xue, Z. L. *CrystEngComm* **2010**, *12*, 1153−1158.

(25) Shibuya, M.; Miyauchi, M. *Chem. Phys. Lett.* **2009**, *473*, 126−130.

(26) Zhang, Y.; Chen, Y. G.; Liu, H.; Zhou, Y. Q.; Li, R. Y.; Cai, M.; Sun, X. L. *J. Phys. Chem. C* **2009**, *113*, 1746−1750.

(27) Wang, J. M.; Lee, P. S.; Ma, J. *Cryst. Growth Des.* **2009**, *9*, 2293−2299.

(28) Yoo, S. J.; Yun, S. U.; Sung, Y. E.; Ahn, K. S. *J. Power Sources* **2010**, *195*, 5422−5425.

(29) Kida, T.; Nishiyama, A.; Yuasa, M.; Shimanoe, K.; Yamazoe, N. *Sens. Actuator B-Chem* **2009**, *135*, 568−574.

(30) Yang, S. K.; Cai, W. P.; Zhang, H. W.; Xu, X. X.; Zeng, H. B. *J. Phys. Chem. C* **2009**, *113*, 19091−19095.

(31) Zeng, H. B.; Cai, W. P.; Li, Y.; Hu, J. L.; Liu, P. S. *J. Phys. Chem. B* **2005**, *109*, 18260−18266.

(32) Liu, Q. X.; Wang, C. X.; Zhang, W.; Wang, G. W. *Chem. Phys. Lett.* **2003**, *382*, 1−5.

(33) Liu, P. S.; Cai, W. P.; Zeng, H. B. *J. Phys. Chem. C* **2008**, *112*, 3261−3266.

(34) Liang, C. H.; Shimizu, Y.; Masuda, M.; Sasaki, T.; Koshizaki, N. *Chem. Mater.* **2004**, *16*, 963−965.

(35) Hu, J. J.; Zabinski, J. S.; Sanders, J. H.; Bultman, J. E.; Voevodin, A. A. *J. Phys. Chem. B* **2006**, *110*, 8914−8916.

(36) Schuffenhauer, C.; Parkinson, B. A.; Jin-Phillipp, N. Y.; Joly-Pottuz, L.; Martin, J. M.; Popovitz-Biro, R.; Tenne, R. *Small* **2005**, *1*, 1100−1109.

(37) Nath, M.; Rao, C. N. R.; Popovitz-Biro, R.; Albu-Yaron, A.; Tenne, R. *Chem. Mater.* **2004**, *16*, 2238−2243.

(38) Gautam, U. K.; Vivekchand, S. R. C.; Govindaraj, A.; Kulkarni, G. U.; Selvi, N. R.; Rao, C. N. R. *J. Am. Chem. Soc.* **2005**, *127*, 3658−3659.

(39) Yang, G. W. *Prog. Mater. Sci.* **2007**, *52*, 648−698.

(40) Wang, H. Q.; Miyauchi, M.; Ishikawa, Y.; Pyatenko, A.; Koshizaki, N.; Li, Y.; Li, L.; Li, X. Y.; Bando, Y.; Golberg, D. *J. Am. Chem. Soc.* **2011**, *133*, 19102−19109.

(41) Szymanski, J. T.; Roberts, A. C. *Can. Mineral* **1984**, *22*, 681−688.

(42) Chemseddine, A.; Bloeck, U. *J. Solid State Chem.* **2008**, *181*, 2731−2736.

(43) Livage, J.; Henry, M.; Sanchez, C. *Prog. Solid State Chem.* **1988**, *18*, 259−341.

(44) Glemser, O.; Holznage., W; Holtje, W.; Schwarzm., E. *Z. Naturforsch. B* **1965**, *20*, 725−746.

(45) Baker, A. P.; Hodgson, S. N. B.; Edirisinghe, M. J. *Surf. Coat. Technol.* **2002**, *153*, 184−193.

(46) Choi, Y. G.; Sakai, G.; Shimanoe, K.; Miura, N.; Yamazoe, N. *Sens. Actuator B-Chem.* **2002**, *87*, 63−72.

(47) Freedman, M. L. *J. Am. Chem. Soc.* **1959**, *81*, 3834−3839.

(48) Zhou, L.; Zou, J.; Yu, M.; Lu, P.; Wei, J.; Qian, Y.; Wang, Y.; Yu, C. *Cryst. Growth Des.* **2008**, *8*, 3993−3998.

(49) Breedon, M.; Spizzirri, P.; Taylor, M.; du Plessis, J.; McCulloch, D.; Zhu, J.; Yu, L.; Hu, Z.; Rix, C.; Wlodarski, W.; Kalantar-zadeh, K. *Cryst. Growth Des.* **2010**, *10*, 430−439.